BMC Chemical Engineering

RESEARCH ARTICLE Open Access

Noble gas separation by a MOF with one-dimensional channels

Yang Liu[1*], Jing Liu[2] and Jianbo Hu[2]

Abstract

Noble gas separation by microporous materials is a promising alternative to energy-intensive cryogenic distillation method by reducing the separation cost; however, developing novel microporous materials with excellent noble gas separation performance is still challenging due to closing chemical and physical properties among the gases. In this study, we propose to separate the noble gases (He, Ne, Ar, Kr and Xe) utilizing a metal organic framework (MOF), named SIFSIX-3-Zn, with ultra-micron sized 1-dimenssional (1D) channels (3.84 Å). Density functional theory (DFT) calculations reveal that the 1D channels provide significant adsorption potential differences among the noble gas molecules in various sizes: the larger the molecular size, the stronger the adsorption potential. Grand canonical Monte Carlo (GCMC) simulations verify that the MOF exhibits exceptional equilibrium separation performance of noble gases. Remarkably, Xe/He and Xe/Ne adsorption selectivity can be as high as 645 and 596, respectively, at 298 K and 10 kPa. While Xe/Kr selectivity in mixed gas is around 12 with a Xe adsorption amount of about 2.27 mmol/g at 273 K and 100 kPa, making SIFSIX-3-Zn one of the promising materials for equilibrium separation of Xe/Kr mixtures.

Keywords: MOFs, Noble gas, Adsorption, Separation

Background

Noble gases, i.e. helium (He), neon (Ne), argon (Ar), krypton (Kr) and xenon (Xe), play vital roles in our daily lives, ranging from lighting and medicine to cryogenic refrigerants [1]. Ne, Ar, Kr and Xe are commercially produced from air by gas liquefaction followed by cryogenic distillation based on the differences in the boiling points (e.g., 27 K for Ne, 87 K for Ar, 120 K for Kr, and 165 K for Xe) [2], which requires large amount of energy inputs. Therefore, developing novel approaches with lower energy inputs is promising to reduce the separation cost of noble gas production.

One of the promising approaches for low-cost noble gas separation is physisorption onto microporous materials, such as activated carbons (ACs) [3], zeolites [4, 5] and metal organic frameworks (MOFs) [6–11]; however, achieving distinguishable equilibrium adsorption abilities among the noble gases for separation is still challenging. Recently, MOFs with open metal sites at the pore surface have shown excellent performance on Xe/Kr separation due to strong interactions between the Xe molecule and accessible open metal sites in the MOFs, indicating that interaction strength plays vital roles on noble gas separation [1]. Furthermore, by screening 670,000 porous material structures for Xe/Kr separation, Simon et al. suggested that highly selective materials should exhibit pore sizes around that of a Xe atom (3.9 Å) to enhance the interaction strength of Xe [12]. This agrees well with the fundamentals that the adsorption potential of molecules in a porous material can be significantly enhanced when the molecular size and pore size closing to each other due to the overlap of van der Waals (vdW) potentials that the molecule "feeling" from the opposite walls of the pore surface, as called "curvature potential" [13, 14].

The adsorption potential varies from molecules in various sizes and porous materials, e.g. MOFs, with thousands of different topologies [13]. Especially, non-uniform sized pores in a material with intersecting cages (Fig. 1a) usually introduce diverse adsorption potentials to molecules, a drawback to achieve high sorption ability at low pressure range if no functional group exist [13]. Therefore, porous materials with uniform sized 1-dimensional (1D) channels (Fig. 1b) are attractive

* Correspondence: yangliu@chbe.gatech.edu
[1]School of Chemical & Biomolecular Engineering, Georgia Institute of Technology, 311 Ferst Dr. NW, Atlanta, GA 30332, USA
Full list of author information is available at the end of the article

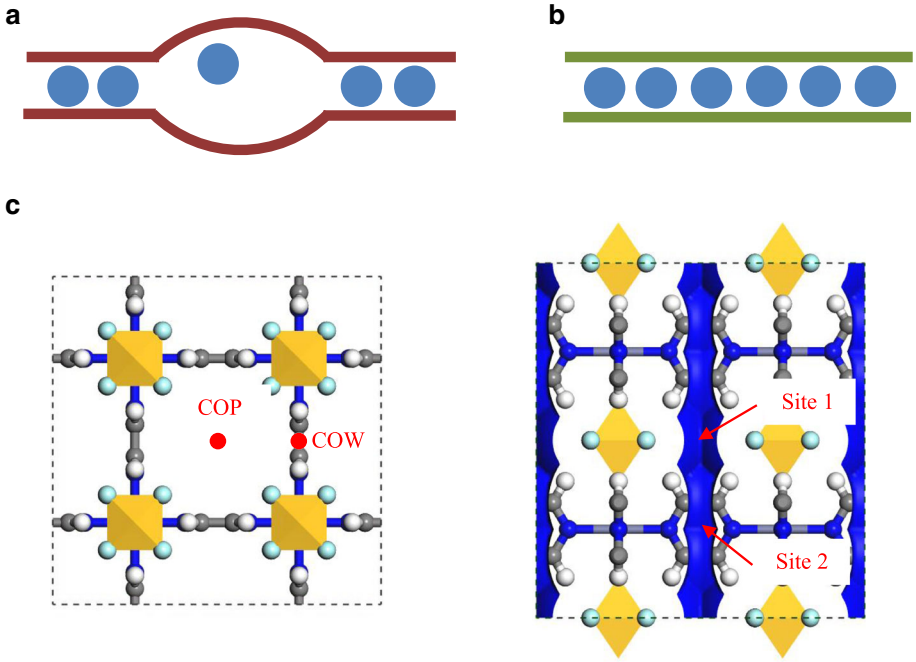

Fig. 1 Schematic representations of (**a**) channels with intersecting cage and (**b**) one-dimensional (1D) channels with uniform size. **c** structure of SIFSIX-3-Zn with specified Site-1 and Site-2 in this work. COP represents the center of the pore, while COW represents the atomic center of the wall atoms. Yellow octahedron: Zn; green ball: Cl; blue ball: N; gray ball: C; and white ball: H

to achieve high adsorption ability by providing strong and uniform adsorption potentials [15] if the channel size is well constrained to angstrom level, such as < 3.9 Å (equals to the molecular size of Xe) for noble gas separation. One of promising porous materials exhibiting such uniform 1D channels is SIFSIX-3-Zn MOF with a channel size of 3.84 Å, closing to the kinetic diameter of Xe (3.9 Å) [16, 17]. Despite the reported slight size difference between the adsorbate (Xe, 3.9 Å) and adsorbent (SIFSIX-3-Zn, 3.84 Å), adsorption of Xe in the MOF is considered in this work as the actual atomic diameter of Xe defined in terms of the size of atom's electron shell is generally smaller than the kinetic diameter. Overall, previous studies have revealed that SIFSIF-3-Zn shows great potentials on capturing CO_2 and C_2H_2 due to the high van der Waals (vdW) potential overlap endowed by the ultra-micron channels and the surrounding basic SF_6^{2-} sites [16, 17]. Here, we demonstrate that the vdW potentials in the 1D channels of SIFSIX-3-Zn vary from noble gas molecules in different sizes, resulting in dramatic differences on gas adsorption abilities in the MOF for effective noble gas separation.

Results and discussion

In SIFSIX-3-Zn, the zinc (II) center is octahedrally coordinated to the four nitrogen atoms of the *pyz* ligands as well as the two SiF_6^{2-} ions (Fig. 1a). In the equatorial plane, the *pyz* ligands bridge the zinc ions to produce grids, while the SiF_6^{2-} groups are coordinated axially and bridge zinc ions, producing an open three-dimensional framework. All *pyz* planes are parallel to the *c*-axis to produce 1D channel, as presented by the blue tubular surface using solvent surface with a radius of 2 Å (Fig. 1b). The 1D channel exhibits overall smooth inner surface with some variations induced by the surface atoms in different atomic radius, which are distinguished by Site-1 nearby the *pyz* ligands and Site-2 nearby the SiF_6^{2-} ions (Fig. 1b).

Density functional theory (DFT) calculations were performed to derive the adsorption potentials of the noble gases inside the channel of SIFSIX-3-Zn, as shown in Fig. 2. Details of the DFT calculations can be found in the Methods. As shown in Fig. 2a and b, the potentials at the two different sites, i.e. Site-1 and Site-2 (Fig. 1b), in the channel are different from each other for all gases. Specifically, the potentials at site-2 surrounded by four *pyz* linkers are much stronger than that of site-1 surrounded by four SiF_6^{2-} ions, indicating that the binding of the noble gases are dominated by vdW interactions, rather than electrostatic interactions with the basic SiF_6^{2-} ions. This agrees well the estimation that strong adsorption/curvature potentials are induced when the molecular size closing to the channel size (3.84 Å), especially for Xe (3.9 Å). The negligible effect of the basic SiF_6^{2-} ions on enhancing the adsorption of noble gases is different from the cases of CO_2 and C_2H_2

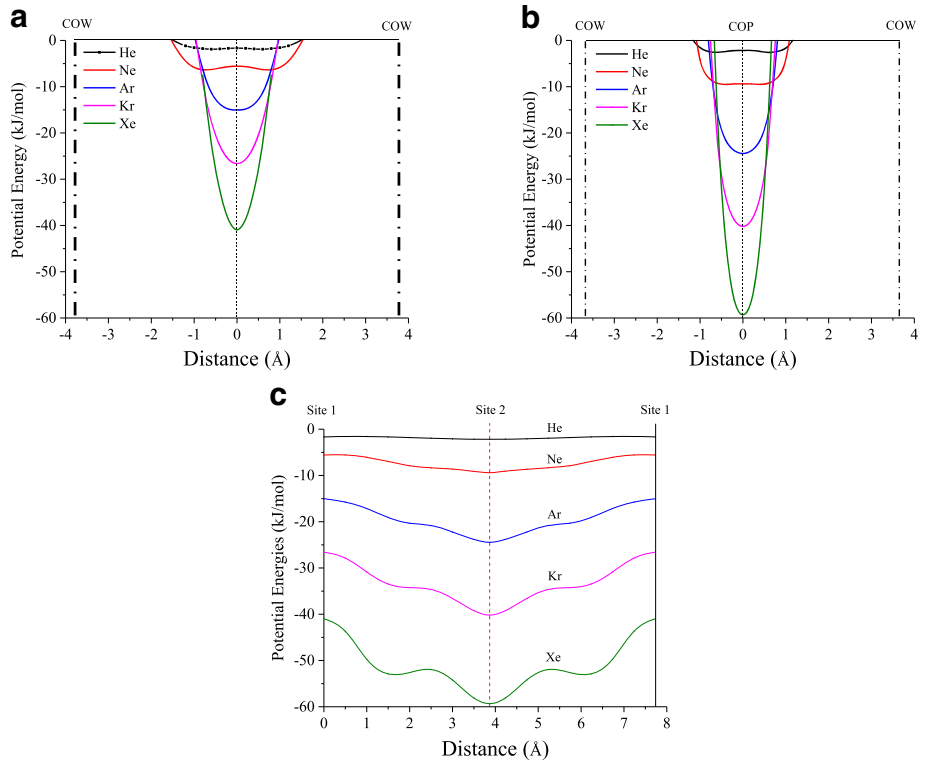

Fig. 2 Potential of noble gases in SIFSIX-3-Zn channel generated by DFT calculations. **a** Site-1; **b** Site-2; and (**c**) from Site-1 to Site-2 along channel direction. COP represents the center of the pore, while COW represents the atomic center of wall atoms

adsorption, in which the SiF_6^{2-} ions significantly enhance the adsorption due to electrostatic interactions. Moreover, the potential energy for the gas molecules show some variations along the channel direction from Site-1 to Site-2 (Fig. 2c) since the channel surface is formed by different atoms (F, C, N and H) with different atomic radius.

The potential curves of He and Ne are different from those of Ar, Kr and Xe because the vdW potentials have no overlap for the smaller molecules (He and Xe) but strong overlap for the bigger molecules (Ar, Kr and Xe), which is further enhanced with the molecular size increases. The highest potential energy of Ar, Kr and Xe at Site-2 are – 25 kJ/mol, – 40 kJ/mol and – 60 kJ/mol, respectively and therefore results in dramatic differences on gas adsorption behaviors in the MOF due to the significant differences on potential energy.

As shown in Fig. 3, grand canonical Monte Carlo (GCMC) simulations confirms that the designated high adsorption selectivity for noble gases is achieved by utilizing the potential energy differences. First of all, the adsorption abilities of the pure noble gases in SIFSIX-3-Zn follows the order of Xe > Kr > Ar > Ne ≈ He (Fig. 3a), agreeing well with the decreasing order of molecular size, i.e. 3.9 Å (Xe), 3.6 Å (Kr), 3.4 Å (Ar), 2.75 Å (Ne) and 2.6 Å (He) (Fig. 3b) as well as the adsorption potentials revealed by DFT calculations (Fig. 2). The isosteric heats of the gases show the same trend (Fig. 3c-d). Remarkably, the adsorption amount of Xe in SIFSIX-3-Zn is about 3.08 mmol/g at 298 K and 100 kPa, a much higher value than those of other gases, i.e. Kr (1.30 mmol/g), Ar (0.54 mmol/g), Ne and He (0.02 mmol/g). Promising adsorption selectivity for Ar/He, Ar/Ne, Kr/He, Kr/Ne, Kr/Ar, Xe/He, Xe/Ne, Xe/Ar and Xe/Kr based on the pure gas adsorption data are found in SIFSIX-3-Zn (Fig. 4). Remarkably, the adsorption selectivity is as high as 645 and 596 for Xe/He and Xe/Ne gas pairs at 298 K and 10 kPa, respectively (Fig. 4a), indicating the SIFSIX-3-Zn with 3.84 Å 1D channels is promising for equilibrium separation of noble gases.

To further elucidate the effects of the curvature potential in the 1D channels of SIFSIX-3-Zn on equilibrium separation of noble gases at different conditions, we performed detailed studies on Xe/Kr separation, one of the most challenging topics in gas separation. Figure 5 shows pure gas adsorption behaviors of Xe and Kr at different temperatures (273 K, 298 K and 313 K) and pressures up to 1000 kPa. The adsorption amounts of both gases increase with the decrease of temperature with a remarkable adsorption amount of Xe of 2.90 mmol/g at 298 K and 100 kPa (Fig. 5a), approximately 73% of the saturation uptake amount of SIFSIX-3-Zn. As results,

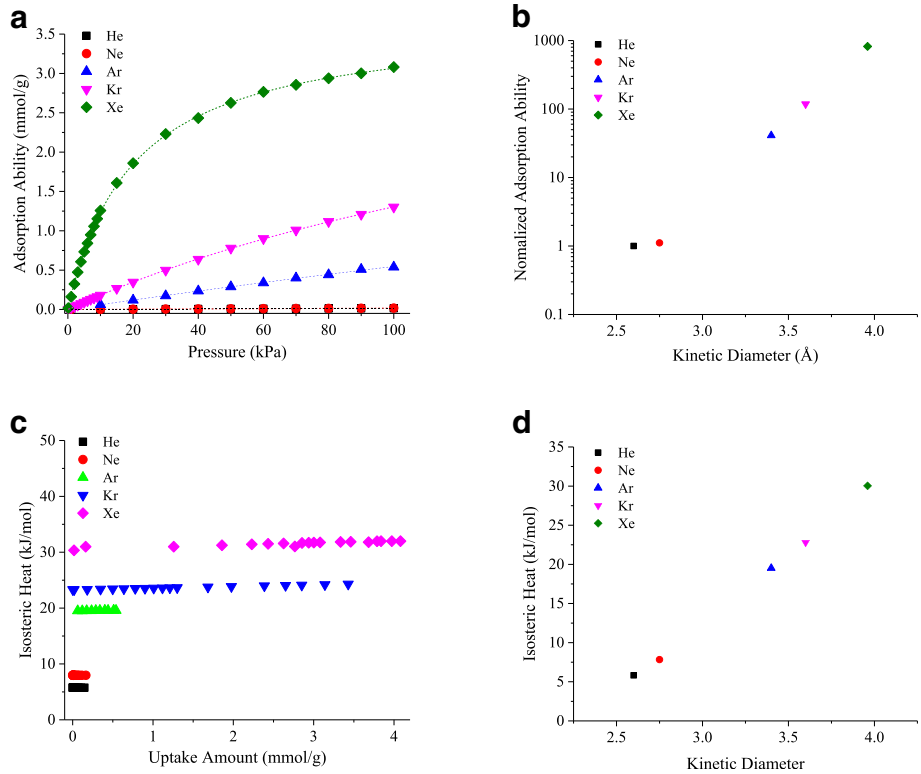

Fig. 3 Adsorption isotherms and isosteric heat of noble gases in SIFSIX-3-Zn by GCMC simulations. **a** adsorption isotherms at 298 K and 0–100 kPa; **b** relationship between normalized adsorption ability (compared to He adsorption amount) and kinetic diameters; **c** isosteric heat and (**d**) relationship between the isosteric heat and kinetic diameters

increasing the pressure from 100 kPa to 1000 kPa shows little improvement on the adsorption amount of Xe due to the limited sites left for sorption, whereas Kr adsorption is dramatically improved (Fig. 5b). Subsequently, the Xe/Kr sorption selectivity based on pure gas sorption data with equal molar concentration (50/50) decreases with the increase of pressure (Fig. 6a); however, Xe/Kr mixture adsorption studies simulating the realistic conditions for Xe/Kr separation interestingly shows no loss of separation performance with pressure change (Fig. 6a). This clearly shows that the strongly adsorbed Xe molecules can always preferentially occupy the sorption sites in SIFSIX-3-Zn and inhibit the adsorption of less favorable Kr molecules, regardless the molar concentration of Kr in the mixture e.g. 20/80 or 50/50 (Fig. 6a). Moreover, lowering the sorption temperature from 298 K to 273 K in mixed gas with a molar concentration of 20/80 (Xe/Kr) can dramatically enhance the Xe

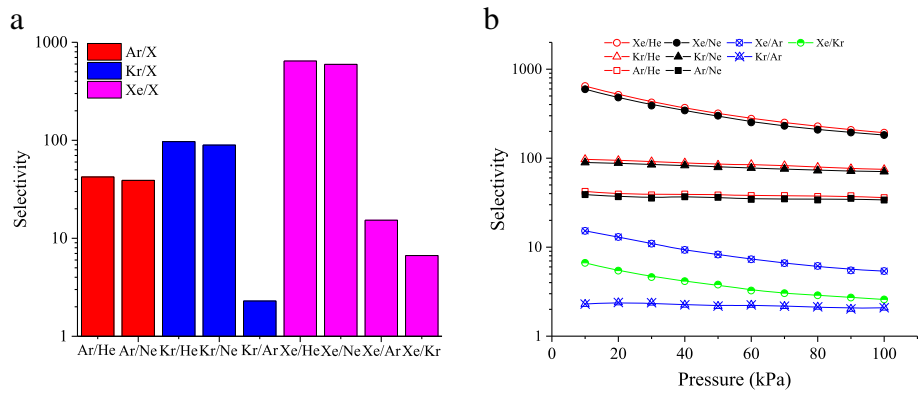

Fig. 4 Equilibrium selectivity of SIFSIX-3-Zn based on pure gas adsorption data at 298 K: **a** 10 kPa, and (**b**) 10–100 kPa

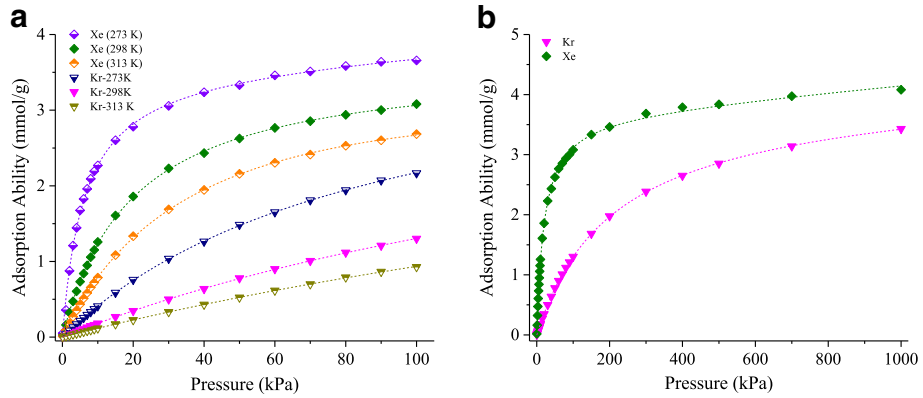

Fig. 5 Xe and Kr uptake isotherms in SIFSIX-3-Zn (**a**) at different temperatures (273 K, 298 K and 313 K) and 0–100 kPa; and (**b**) at 298 K and 0–1000 kPa

adsorption and Xe/Kr selectivity (Fig. 6a), again, owing to the favorable adsorption of Xe over Kr in the SIFSIX-3-Zn framework (Fig. 6b). Overall, the well-maintained adsorption selectivity in mixed gas conditions demonstrates that SIFSIX-3-Zn is a promising material for Xe/Kr separation.

To evaluate the potential of the identified MOF with strong curvature potential, the separation efficiencies (Xe/Kr selectivity vs Xe adsorption amount) of SIFSIX-3-Zn in mixed gas conditions (20/80) are further compared with other MOFs (Fig. 7). At 298 K and 100 kPa, the Xe/Kr separation efficiency of SIFSIX-3-Zn is comparable to that of NiMOF-74, and greatly surpasses those of CuBTC and IRMOF-1. Remarkably, the Xe/Kr separation efficiency of SIFSIX-3-Zn overcomes all the porous materials reported by far by simply decreasing the sorption temperature from 298 K to 273 K, a much less challenging operation temperature comparing with cryogenic distillation method (<< 165 K). Therefore, equilibrium separation of Xe/Kr using SIFSIX-3-Zn at lower temperatures (e.g. sub-ambient temperature, but still much higher than that in cryogenic distillation conditions) could be a promising approach to balance the separation efficiency and energy input, maximizing the overall Xe/Kr separation efficiency. This is similar with the idea to separate CO_2/CH_4 using a hybrid separation process combining membrane with low temperature system; however, detailed studies involving capital investments evaluation and operation temperature optimization are required in future [18].

Conclusions

In conclusion, we have demonstrated that noble gases can be efficiently separated by the equilibrium separation method utilizing the curvature potential difference of the gas molecules in the well-chosen SIFSIX-3-Zn MOF with ultra-micron sized 1D channels. Future works will focus on further revealing the relationship between the separation efficiency and 1D channel sizes for different noble gas pairs, and screening more MOF materials with 1D channels for the application. Experimental verifications of the prediction results based on theoretical understandings and simulations are also required in future works.

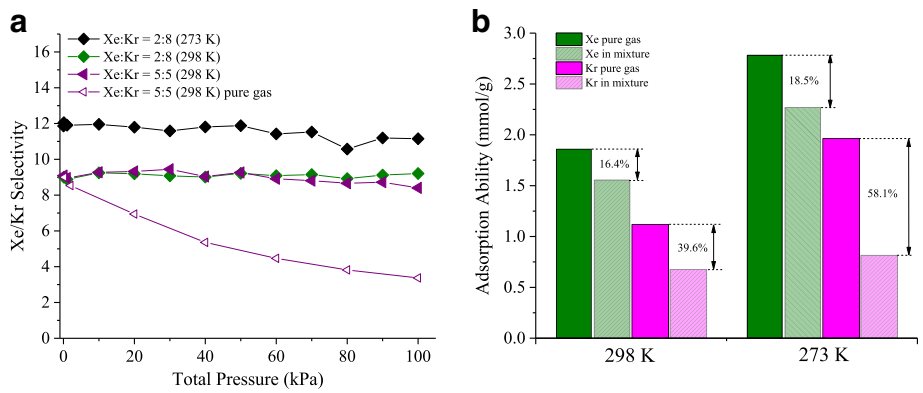

Fig. 6 **a** Xe/Kr equilibrium selectivity in mixed gas conditions (molar fraction: 20/80 and 50/50) at different temperatures (273 K and 308 K). **b** comparison of the adsorption ability of Xe and Kr in mixed gas and pure gas conditions with molar fraction of 20/80 at 100 kPa

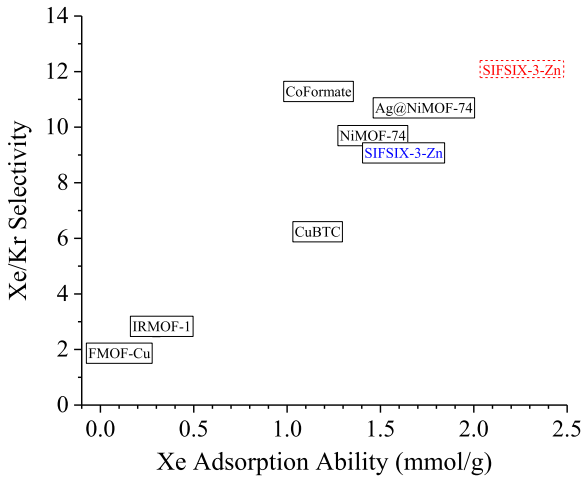

Fig. 7 Comparison of the Xe/Kr (20/80) separation efficiency of various MOFs at 298 K and 100 kPa. The data of SIFSIX-3-Zn obtained in our simulations are plotted as red (273 K) and blue (298 K)

Methods

Density functional theory calculations

The structure of SIFSIX-3-Zn was constructed from the experimental XRD data [16]. The potential energies for noble gas molecules in the channel of SIFSIX-3-Zn were calculated by the DFT method based on hundreds of configurations for each gas molecule. Specifically, the gas molecule is manually moved from center of the channel to the wall at one side of the channel with a step distance of 0.1 Å to generate the configurations for the molecule by considering different site, Site-1 and Site-2. The potential energy (PE) was calculated for each configuration to generate the final potential curve using the following equation:

$$PE = E(AB) - (E(A) + E(B)) \quad (1)$$

where E(A) is the zero-point energy of the adsorbate, E(B) is the zero-point energy of the substrate, and E(AB) is the zero-point energy of the adsorbate/substrate system. The potentials along the channel direction were generated using the same method based on configurations by placing the gas molecule Site-1 initially and moved toward to Site-2 with a step distance of 0.5 Å.

The periodic boundary condition was considered in all calculations. The Becke exchange plus Lee-Yang-Parr correction (BLYP) exchange-correlation functional [19] with double numeric polarization (DNP) basis set [20] and DFT semicore pseudopots (DSPP) are used. A real-space orbital global cutoff of 4.0 Å was applied, and the convergence threshold parameters for the optimization were 2×10^{-5} (energy), 4×10^{-3} (gradient), and 5×10^{-3} (displacement), respectively. To further improve the accuracy of the results, Grimme method for DFT-D approach, which is a semi-empirical combination of DFT approach with pairwise corrections, were used [21].

Force field

Conventional Universal force field was used in this work. The interaction of gas-adsorbent and gas-gas were modeled as a combination of site-site Lennard-Jones (LJ):

$$u_{ij}(r) = \sum_{\substack{\alpha \in i \\ \beta \in j}} \left\{ 4\varepsilon_{\alpha\beta} \left[\left(\frac{\sigma_{\alpha\beta}}{\gamma_{\alpha\beta}} \right)^{12} - \left(\frac{\sigma_{\alpha\beta}}{\gamma_{\alpha\beta}} \right)^{6} \right] \right\} \quad (2)$$

where ε_0 is the permittivity of the vacuum, and $\sigma_{\alpha\beta}$ and $\varepsilon_{\alpha\beta}$ are the collision diameter and well depth, respectively. The LJ cross-interaction parameters were determined by the Lorentz-Berthelot mixing rules.

Grand canonical Monte Carlo (GCMC) simulation

A 8 × 8 × 8 unit cell system of SIFSIX-3-Zn with periodic boundary conditions applied in all three dimensions were constructed, and the framework was treated as rigid with atoms frozen at their crystallographic positions during GCMC simulations. As previously described, the cutoff radius for the LJ interactions was set to 12 Å. For each state point, GCMC simulation consists of 1.0×10^7 steps to guarantee the equilibration, followed by additional 1.0×10^7 steps to sample the desired thermodynamics properties. The following equation was used to define the selectivity for component A relative to component B: $S = (\alpha_A/\alpha_B)(\beta_A/\beta_B)$, where α and β are the molar fractions of the components in the adsorbed and gas phases, respectively.

Acknowledgements
Not applicable.

Funding
This work is supported by National Natural Science Foundation of China (51676079). The funders had no role in study design, data collection and analysis, interpretation of data, or preparation of the manuscript.

Availability of data and materials
Not applicable.

Authors' contributions
YL performed the DFT and GCMC simulations. YL, JL and JH discussed the findings in this paper. YL coordinated the writing of the paper, and all authors contributed to revising the paper. All authors read and approved the final manuscript.

Competing interests
The authors declare that they have no competing interests.

Publisher's Note

Author details
[1]School of Chemical & Biomolecular Engineering, Georgia Institute of Technology, 311 Ferst Dr. NW, Atlanta, GA 30332, USA. [2]State Key Laboratory of Coal Combustion, Huazhong University of Science and Technology, Wuhan 430037, China.

Received: 17 October 2018 Accepted: 2 January 2019
Published online: 30 January 2019

References

1. Banerjee D, Cairns AJ, Liu J, Motkuri RK, Nune SK, Fernandez CA, Krishna R, Strachan DM, Thallapally PK. Potential of metal-organic frameworks for separation of xenon and krypton. Acc Chem Res. 2015;48:211–9.
2. Ryan P, Farha OK, Broadbelt LJ, Snurr RQ. Computational screening of metal-organic frameworks for xenon/krypton separation. AIChE J. 2011;57:1759–66.
3. Kuznetsova TA, Tolmachev AM, Kryuchenkova NG, Firsov DA, Fomkin AA. Thermodynamics of adsorption of krypton, xenon, nitrogen, and oxygen on microporous active carbon at temperatures above critical values. Prot Met Phys Chem Surf. 2013;49:367–72.
4. Lawler KV, Sharma A, Alagappan B, Forster PM. Assessing zeolite frameworks for noble gas separations through a joint experimental and computational approach. Microporous Mesoporous Mater. 2016;222:104–12.
5. Hye Kwon Y, Kiang C, Benjamin E, Crawford P, Nair S, Bhave R. Krypton-xenon separation properties of SAPO-34 zeolite materials and membranes. AIChE J. 2017;63:761–9.
6. Liu J, Thallapally PK, Strachan D. Metal-organic frameworks for removal of Xe and Kr from nuclear fuel reprocessing plants. Langmuir. 2012;28:11584–9.
7. Thallapally PK, Grate JW, Motkuri RK. Facile xenon capture and release at room temperature using a metal-organic framework: a comparison with activated charcoal. Chem Commun. 2012;48:347–9.
8. Bae YS, Hauser BG, Colon YJ, Hupp JT, Farha OK, Snurr RQ. High xenon/krypton selectivity in a metal-organic framework with small pores and strong adsorption sites. Microporous Mesoporous Mater. 2013;169:176–9.
9. Magdysyuk OV, Adams F, Liermann HP, Spanopoulos I, Trikalitis PN, Hirscher M, Morris RE, Duncan MJ, McCormick LJ, Dinnebier RE. Understanding the adsorption mechanism of noble gases Kr and Xe in CPO-27-Ni, CPO-27-mg, and ZIF-8. Phys Chem Chem Phys. 2014;16:23908–14.
10. Chen X, Plonka AM, Banerjee D, Krishna R, Schaef HT, Ghose S, Thallapally PK, Parise JB. Direct observation of Xe and Kr adsorption in a Xe-selective microporous metal-organic framework. J Am Chem Soc. 2015;137:7007–10.
11. Lee SJ, Yoon TU, Kim AR, Kim SY, Cho KH, Hwang YK, Yeon JW, Bae YS. Adsorptive separation of xenon/krypton mixtures using a zirconium-based metal-organic framework with high hydrothermal and radioactive stabilities. J Hazard Mater. 2016;320:513–20.
12. Simon CM, Mercado R, Schnell SK, Smit B, Haranczyk M. What are the best materials to separate a xenon/krypton mixture? ChemMater. 2015;27:4459–75.
13. Xiao J, Wei J. Diffusion mechanism of hydrocarbons in zeolites-I. Theory. Chem Eng Sci. 1992;47:1123–41.
14. Everett DH, Powl JC. Adsorption in slit-like and cylindrical micropores in the henry's law region. A model for the microporosity of carbons. J Chem Soc. Faraday Trans. 1976;72:619–36.
15. Liu Y, Zhang B, Liu D, Sheng P, Lai Z. Fabrication and molecular transport studies of highly c-oriented AFI membranes. J Membr Sci. 2017;528:46–54.
16. Nugent P, Belmabkhout Y, Burd S, Cairns AJ, Luebke R, Forrest K, Pham T, Ma S, Space B, Wojtas L, Eddaoudi M, Zaworotko MJ. Porous materials with optimal adsorption thermodynamics and kinetics for CO_2 separation. Nature. 2013;495:80–4.
17. Cui X, Chen K, Xing H, Yang Q, Krishna R, Bao Z, Wu H, Zhou W, Dong X, Han Y. Pore chemistry and size control in hybrid porous materials for acetylene capture from ethylene. Science. 2016;353:141–4.
18. Liu Y, Liu G, Zhang C, Qiu W, Yi S, Chernikova V, Chen Z, Belmabkhout Y, Shekaha O, Eddaoudi M, Koros W. Enhanced CO_2/CH_4 separation performance of a mixed matrix membrane based on tailored MOF-polymer formulations. Adv Sci. 2018;5:1800982.
19. Becke AD. A multicenter numerical integration scheme for polyatomic molecules. J Chem Phys. 1988;88:2547.
20. Delley B. From molecules to solids with the $DMol^3$ approach. J Chem Phys. 2000;113:7756.
21. Asmadi A, Neumann MA, Kendrick J, Girard P, Perrin MA, Leusen FJ. Revisiting the blind tests in crystal structure prediction: accurate energy ranking of molecular crystals. J Phys Chem B. 2009;113:16303.